Hindawi
Geofluids
Volume 2022, Article ID 5368690, 18 pages
https://doi.org/10.1155/2022/5368690

Research Article

Study on Seepage Characteristics of Radial Flow in Rock Mass Based on Radius Effect

Kaichen Liu, Junrui Chai, Yao Zhang, Ying Tian, and Ruiqing Li

State Key Laboratory of Eco-Hydraulics in Northwest Arid Region, Xi'an University of Technology, Xi'an 710048, China

Correspondence should be addressed to Junrui Chai; jrchai@xaut.edu.cn

Received 15 September 2021; Revised 1 January 2022; Accepted 12 January 2022; Published 30 January 2022

Academic Editor: Yong Liu

The radial fluid flow in fractures is affected by the size of the inner diameter and the position of the outer diameter, but the influence of the two factors on the flow velocity remains unclear. This study reveals the relationship through the coupled shear flow experiments and numerical simulations. Experimental results show that the fracture aperture is decreased by 0.175 mm under the unit effective stress, with the increase of 0.902 MPa in the shear stress. COMSOL is used to simulate the seepage of fractures under different inner and outer diameters. Simulation results show that the transition from nonlinear to linear flow occurs in the radial direction when the hydraulic pressure is 0.2 and 0.4 MPa, and the positions of linear flow are 42 mm and 71 mm. The effect of the fracture surface results in a stratified flow velocity when the fluid flow enters the fracture aperture. Increasing the inner diameter raises the flow rate but decreases the maximum flow velocity. The maximum velocity difference can be as much as three times when the inner diameter difference is 6 mm. The seepage width of radial flow has a nonlinear relationship with the inner and outer diameters. The growth rate of the seepage width decreases as the ratio of the outer to the inner diameter increases. The modified cubic law considering the radius effect is proposed to improve the calculation accuracy of radial flow.

1. Introduction

Single fracture and fracture network are basic forms in rock masses, and the existence of fractures significantly affects the mechanical and hydraulic behaviors [1–3]. The permeability of fractures is generally several orders of magnitude larger than that of the matrix; thus, the fluid flow mainly occurs in the fractures. Moreover, the stability of rock mass relies on hydraulic properties. The hydromechanical behaviors in fractures play an important role in the control of groundwater flow and solute transport, the repair of hazardous dissolved pollutants, and the long-term storage of underground nuclear waste [4–6]. The present researches mostly focus on the variation of geometrical properties caused by mechanical loads (i.e., normal and shear loads) and the resulting change in hydraulic properties. The increase in the normal loads can decrease the flow path due to the increased contacts of fracture surfaces [5, 7, 8], and the asperities may be crushed under the effect of high normal stress, resulting in secondary particles that can further influence the flow channel [9]. The effect of shear loads can lead to the relative displacement between the upper and lower fracture walls. The variation of interior geometries as the shear displacement increases is determined by many factors such as roughness, mechanical properties of the fracture surface, and infillings [10], and the hydraulic conductivity may exhibit multiple variations [8, 11–13]. Shear dilation of fractures is inhibited by the increase in normal stress due to the combined effect of normal and shear stresses, and the two factors have completely different effects on the variation of fracture aperture [14, 15]. The damage of the fracture surface is a key factor in the hydromechanical behaviors [16, 17].

The Reynolds number is widely used to evaluate the flow regime under different geometrical and hydraulic properties [18, 19]. The fluid flow is in the linear flow regime and the cubic law is applicable when the Reynolds number is relatively low. However, the inertial effect cannot be ignored compared with the viscous effect when the Reynolds number is relatively high; a nonlinear relationship between flow rate

and the hydraulic gradient is observed at this time, and the cubic law may be invalid [20–22]. The fluid flow in fractures can be effectively simulated by considering the heterogeneous apertures due to the tortuous flow channels caused by surface roughness [23–25]. Wang et al. [26] considered the local tortuosity and roughness effects in fractures and proposed a modified local cubic law. Many scholars have modified the cubic law by considering the effects of roughness, contacts, and fracture fillings. However, most of the existing studies are performed under a small shear displacement, and the correlation analysis of shear stress, fracture aperture, and fluid flow in the complete shear process is insufficient.

The flow mode in fractures is usually divided into parallel and radial flows due to the difference in water inlet and outlet positions and streamline forms. The former has been widely investigated, while the latter lacks relevant investigations. The radial flow mode has a wide range of applications in practical engineering. For example, the radial flow is a common flow pattern in oil reservoir systems, in which the streamlines converge at a common center in two dimensions [27]; the groundwater flows from the surrounding rock to the underground tunnel in a radial flow regime when the tunnel is excavated [28]; analysis of the hydraulic pressure of the leakage force in the drainage chamber usually assumes that the flow direction is radially symmetrical [29].

In the process of radial fluid flow, the increase in the radial distance leads to constant change in seepage width, which complicates the calculation of flow velocity, flow regime, and flow rate. Existing studies have found that the effective permeability decreases with the increasing radial distance near the wellbore [3, 27, 30, 31]. Changjun and Zhenchun [32] derived the expression of the critical radius, which can accurately describe the distribution of groundwater based on Forchheimer and exponential equations. Zareifard Mohammad and Fahimifar [29] further proposed the expression of the influence radius and stress distribution. Zhang et al. [33] investigated the velocity distribution along the radial distance in two-dimensional radial flow fractures. Most of these studies focus on the permeability in macroscopic fractures, but the variation of the flow regime along the radial distance in three-dimensional fractures and the influence of the inner diameter on the fracture seepage are disregarded. The seepage width has no unified expression when the cubic law derived from the parallel flow is applied to radial flow, and a large error exists with the application. The quantitative relationship among seepage width, inner diameter, and outer diameter requires further investigation.

Therefore, this study first investigated aperture variation and fracture surface damage under different conditions through laboratory experiments and analyzed the shear stress during the complete shearing process. The numerical simulations were performed on the basis of aperture data from experiments to simulate radial fluid flow in three-dimensional fractures, and the influence of internal and external diameters on fracture flow patterns was analyzed. Finally, the modified cubic law in the radial flow regime is obtained with the identified relationship among seepage width, inner diameter, and outer diameter.

2. Shear Test

2.1. Test Instrument and Specimen. At present, researches on fracture seepage are mostly based on laboratory tests, because laboratory tests can well control the influencing factors brought by the environment and have the advantages of simplicity and convenience. To repeat the test and simplify the test operation, gypsum specimens were used for testing. The shear process of the specimen is used to simulate the change of the fracture aperture. The coupled shear flow experiment is carried out on TJXW-600, a hydromechanical coupling test system, as shown in Figure 1. The key part is the shear box shown in Figure 2. The upper and lower test specimens are put into the shear box, and the center of the lower test specimen has a water inlet with a diameter of 8 mm. The flow enters the fracture from the water inlet and flows radially toward the outlet. There is a water outlet on the surface of the lower shear box, which is responsible for collecting the fluid in the fractures. The horizontal force is applied to the upper specimen, pushing the specimen to complete the shearing process.

The use of small-scale rock samples in the experiment will overestimate the strength of the intact rock, and artificial specimens can solve this problem to a certain extent [34]. We mixed gypsum powder, water, and retarder in a mass ratio of 1 : 0.25 : 0.005 and poured the gypsum mixture into the mold to fabricate test specimens with different roughness. The smooth fracture surface is shown in Figure 2(b), and the rough fracture surface is shown in Figure 2(c). The height of the test specimen is 75 mm and the diameter is 200 mm. The mechanical performance parameters tested through the mechanical tests are recorded in Table 1. It is found that the specimens used can simulate the sandstone shearing process well within a certain range.

2.2. Test Scheme. This paper mainly studies the influence of hydraulic pressure and normal stress on the fracture aperture, shear stress, and fluid flow. The test is divided into 3 parts. The first part studies the influence of different normal stresses on fluid flow, and the normal stress increases from 1.27 MPa to 2.55 MPa. The second part studies the influence of different hydraulic pressures on fluid flow, and the hydraulic pressure increases from 0 MPa to 0.8 MPa. The third part is a comparative test, which uses a rough fracture surface to study the change process of shear stress. The specific test parameters and test plan are shown in Table 2.

At the beginning of the test, the test specimen is put in the shear box and the sealing condition of the rubber ring is checked. Then the normal stress is applied, and the water is introduced after the stress is stable. In order to ensure the stability of the pressure gradient in the shearing process, the shear process is carried out after the flow is stabilized for 2 minutes. The test is finished when the shear reaches 32 mm.

Due to the compression of the normal stress and the dilation of the shearing, the aperture of the fracture will change. During the test, the fracture aperture was measured using the displacement meter shown in Figure 1. Since the lower specimen is fixed, the position of the lower fracture

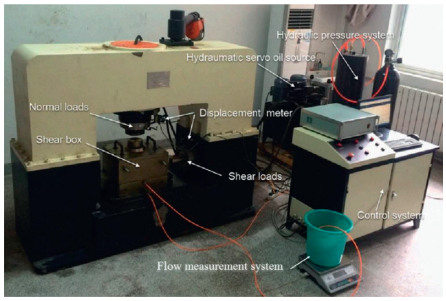

Figure 1: TJXW-600 hydromechanical coupling test system.

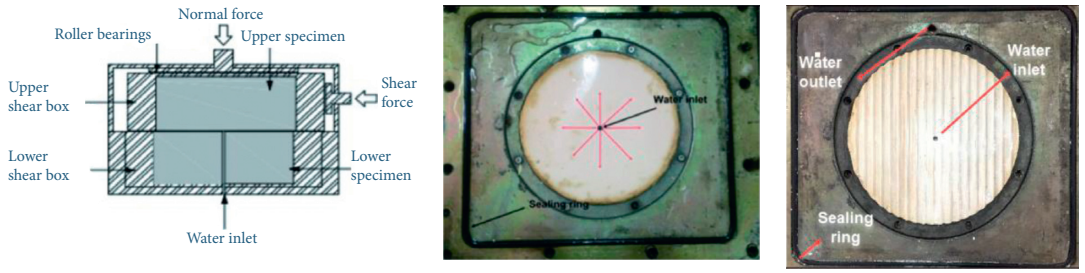

(a) (b) (c)

Figure 2: Schematic figure of shear box internal structure and specimen assembly. (a) Shear box internal structure. (b) Smooth specimen surface. (c) Rough specimen surface.

Table 1: Mechanical property parameters of specimens.

Physical and mechanical parameters	Unit	Experiment material	Sandstone
Density	g/cm^3	2.066	2.24~2.77
Compressive strength	MPa	38.8	20~200
Modulus of elasticity	GPa	28.7	10~100
Poisson's ratio		0.23	0.2~0.3
Cohesive	MPa	5.3	8~40
Internal friction angle	°	60	35~50

Table 2: Test conditions description.

Test group	1	2	3	4	5	6	7	8	9	10	11
Normal stress (MPa)	1.27	1.59	1.91	2.23	2.55			1.91			1.91
Hydraulic pressure (MPa)			0.6			0	0.2	0.4	0.6	0.8	0.6
Shear rate (mm/min)						15					

surface remains unchanged during the shearing process. The displacement meter can record the normal displacement of the upper fracture surface at any shear position. The variation of fracture aperture is the difference between the normal displacement at any position and the initial normal displacement. The actual aperture of the fracture at any position is equal to the sum of the change in aperture and the initial aperture. The flow measurement system shown in Figure 1 directly records the cumulative flow. The recorded water mass needs to be converted into volume based on the water density at room temperature. In order to obtain the instantaneous flow rate at any position during the shearing process, we choose 1 mm shear displacement as the basis of calculation, and the instantaneous flow rate can be calculated by using the ratio of accumulated flow rate to time.

3. Radial Flow Analysis

In this study, the variation of fracture aperture and the failure of fracture structures under different normal stress and hydraulic pressure are simulated through shear test. At the same time, the software is used to simulate the fluid flow under different inlet and outlet radii and the velocity distribution inside the fracture under different hydraulic pressures. Since the flow recorded directly in the test is the cumulative flow, which cannot directly reflect the change of the flow, the instantaneous flow at different shear displacements should be calculated.

3.1. Shear Stress Analysis. At present, most studies on fracture seepage are based on the mechanical and hydraulic

behaviors. The change of stress field in the shearing process is mainly reflected in the change of shear stress. We have plotted the shear stress change process for groups 1–10. Considering that the change processes of shear stress in the 10 groups are similar, this study mainly analyzes the shear stress change process under 1–5 groups of tests.

The dashed-dotted line in Figure 3 shows the shear stress change process of tests 1–5, and the red line in the figure shows the shear stress change process of test 11. Test 11 was carried out as a comparative test, with the purpose of analyzing the difference in shear stress changes under different roughness. The shear stress curves under different normal stresses show obvious stratification. The fracture surface used in this study is relatively smooth. Therefore, it is different from the shear stress change process under large roughness. The shear stress change process can be divided into three stages according to the shear stress peak value and shear stress valley value: (1) In the first stage, with the progress of shearing, the surfaces of the upper and lower specimens are in close contact and improved matching under small roughness. With the progress of shearing, the surface of the specimen is gradually destroyed, accompanied by the generation of debris, which increases the friction force and shear stress. (2) When the shear stress reaches the shear peak, a large failure occurs on the specimen surface, and the matching degree and friction coefficient between the upper and lower specimens decrease, making the shear stress gradually decrease in the second stage and reach the shear stress valley value. (3) In the third stage, as the shear continues, the broken asperities on the fracture surface increase and become smaller particles with further shearing, which increases the upper and lower friction coefficients. Therefore, the shear stress gradually increases with the continuous shearing. The shear process for two fractures with different roughness is shown in Figure 3, and the red curve represents the change of shear stress on the rougher fracture surface. After comparative analysis, it can be seen that the matching degree of rougher fracture surfaces is not high, and the fracture surfaces are further matched under shearing. Therefore, the shear stress increases slowly in the initial stage. However, after the peak shear stress, due to the failure of the upper and lower asperities, the blocking effect between the upper and lower specimens suddenly disappeared, so the shear stress would suddenly decrease in a small range. The shear stress of relatively smooth fractures decreases slowly. Moreover, due to the different effects of the residual failure after the surface failure of the specimen, the shear stress shows two different trends of decreasing and increasing with the continuous shearing. Because the roughness affects the destruction of the fracture surface, after the peak shear stress, the shear stress of the rough fracture and the smooth fracture shows two different trends of decreasing and increasing, respectively. These differences in shear stress variations are ascribed to the effect of surface roughness [35]. Therefore, when analyzing the shear stress in the fracture, we should choose the suitable model according to different roughness.

In the quantitative analysis of shear stress in the shearing process, it is found that there are obvious differences between the peak shear stress and the valley shear stress under different normal stresses. When analyzing the stress characteristic value under different hydraulic pressure, the outward dilation of the fracture is caused by the hydraulic pressure, which counteracts part of normal stress. In the analysis of peak shear stress and valley shear stress, the effect of hydraulic pressure should be taken into account, and the effective stress σ_e should be used instead of the normal stress. The expression of effective stress is

$$\sigma_e = \sigma_n - \sigma_w. \tag{1}$$

Therefore, the relationship between the shear stress value and the effective normal stress under different working conditions is recorded in Table 3.

The test data are plotted in Figure 4, and the relationship among data points in the figure obviously shows a linear relationship. The variation trend between peak shear stress and valley shear stress shows an obvious consistency. The fitting relation of peak shear stress is as follows:

$$y = 0.059 + 0.902x. \tag{2}$$

The fitting relation of valley shear stress is

$$y = 0.022 + 0.775x. \tag{3}$$

When the effective stress increases by 1 MPa, the peak shear stress increases by 0.902 MPa, and the valley shear stress increases by 0.775 MPa. We can infer that the internal friction angle of the fracture surface is reduced to 42.05° under the action of fluid flow infiltration.

3.2. Fracture Aperture Analysis. The influence of external load on fracture affects the shear stress during failure process and the fracture aperture. The fracture aperture and the degree of zigzag of the fracture determine the change of the flow channel. This paper mainly studies the change of fracture aperture under normal pressure and water pressure and analyzes the change of flow rate during the shearing process. In the test process, the initial fracture aperture is u_0; the fracture aperture will be compressed under normal stress, and the variation is recorded as u_n. In the hydraulic action, the fracture surface dilation is outward, and the resulting aperture change is recorded as u_w. In the shearing process, the change of fracture aperture caused by dilation caused by the relative movement between the upper and lower specimens is recorded as u_τ, and the deformation of the upper and lower fracture planes due to the compression of normal stress is recorded as Δu. Therefore, the actual fracture aperture e at any displacement was

$$e = u_0 - u_n + u_w + u_\tau - \Delta u. \tag{4}$$

After the specimen assembly, the initial, normal stress and fracture aperture changes measured by displacement sensor are recorded. The computer directly records the change of vertical displacement, and the fracture aperture at any shear displacement is calculated from the difference of vertical displacement. The deformation generated by stress compression can be calculated by the following equation:

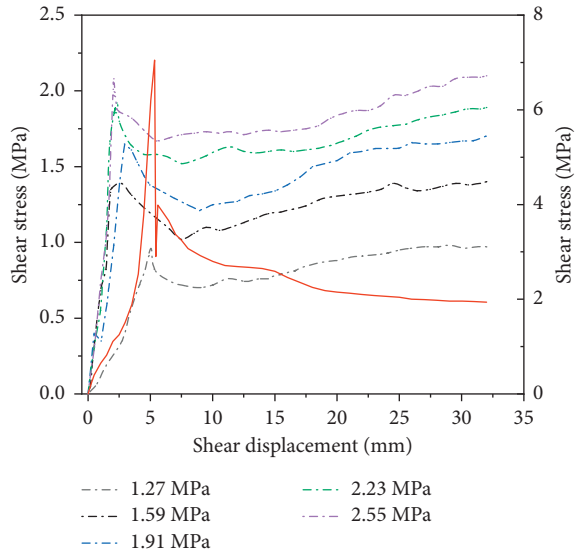

Figure 3: Curve of shear stress during shear process.

Table 3: The shear stress peak value and shear stress valley value under different working conditions.

Test	1	2	3	4	5	6	7	8	9	10
Effective stress σ_e (MPa)	1.07	1.39	1.71	2.03	2.35	1.91	1.84	1.78	1.71	1.64
Peak shear stress (MPa)	0.96	1.39	1.65	1.92	2.08	2.67	1.84	1.74	1.65	1.52
Valley shear stress (MPa)	0.7	1.02	1.21	1.52	1.67	1.96	1.35	1.32	1.21	1.12

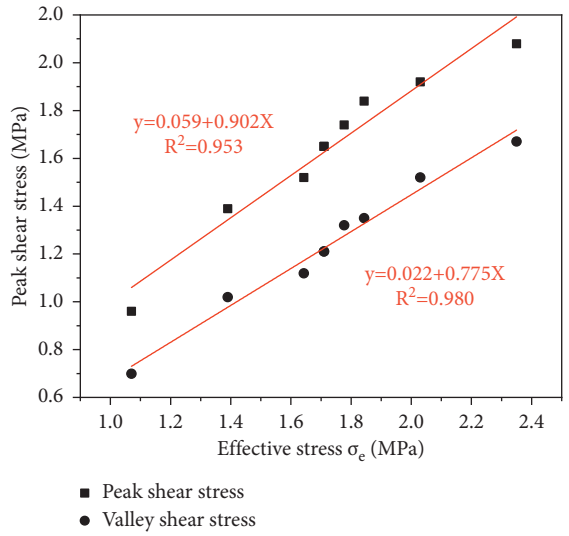

Figure 4: Fitting curve of stress eigenvalue relation.

$$\Delta u = \frac{\sigma_n l}{EA}, \tag{5}$$

where σ_n is normal pressure (kN), l is specimen's height (mm), E is elastic modulus (GPa), and A is specimen's cross-sectional area (mm). The maximum normal deformation is 0.007 mm, which is about 1/50 of the change of fracture width, so the compression deformation of the specimen can be ignored in this study.

We plotted the change of fracture aperture of groups 1–5 and groups 6–10 in Figures 5 and 6. The change of fracture aperture of relatively smooth fracture during shear can be divided into three stages. In the first stage, within the small shear displacement range, the aperture remains unchanged. The reason may be that the shear stress does not reach the state of failure of the fracture surface at the beginning of shearing. There is no debris in the fracture, so the fracture aperture does not change. Then, due to the gradual increase

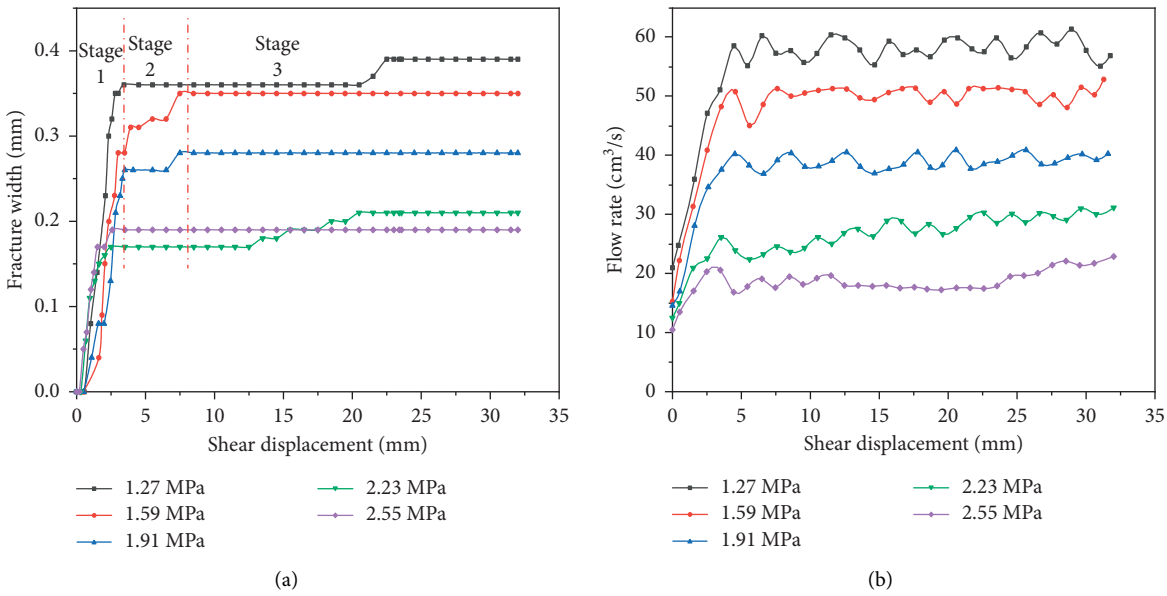

Figure 5: Flow rate and fracture aperture curve under different normal stress rates.

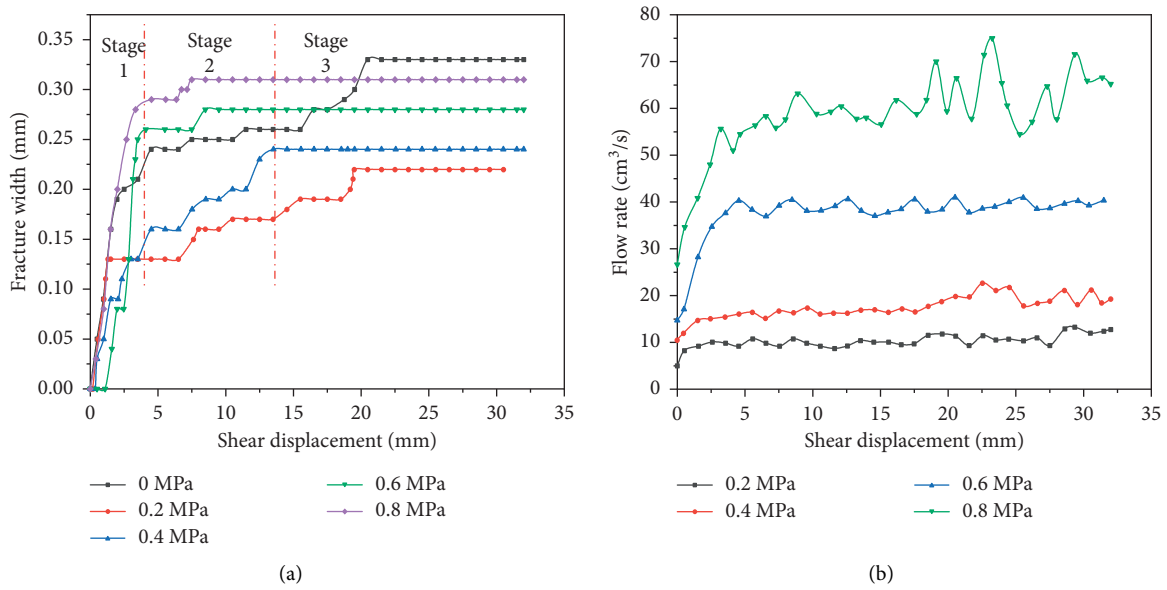

Figure 6: Flow rate and fracture aperture curve under different hydraulic pressure rates.

of shear stress, the structural plane began to fail, and the resulting debris between the upper and lower specimens led to a rapid increase in fracture aperture. The second stage is the small adjustment stage; the volume and size of the broken material produced become homogeneous under the shearing and the compression under normal stress. In the third stage, the fracture aperture tends to be uniform and the height is basically similar during the subsequent shear process, so the variation remains stable. Obviously, the larger the normal stress, the smaller the change in fracture aperture, because, under the normal stress, the aperture between the upper and lower specimens will close. Further analysis shows that the increase of normal stress makes the volume of debris particles further broken after the failure of the structural plane, thus reducing the aperture of the fracture. Under the action of hydraulic pressure, the aperture of fracture will increase, but this change is not obvious and is greatly affected by shear failure.

In order to quantitatively analyze the change of fracture aperture, we can calculate the fracture aperture after shear stabilization under different working conditions by using equation (4). The calculated results are recorded in Table 4.

According to the fracture aperture data in the table, the relationship between effective stress and fracture aperture is plotted in Figure 7. It can be seen that the fracture aperture decreases with the increase of effective stress. This is because the contact between the fracture surfaces is compressed and broken under the action of normal stress, and the fracture

Table 4: Fracture aperture under different working conditions.

Test	1	2	3	4	5	6	7	8	9	10
Normal stress (MPa)	1.27	1.59	1.91	2.23	2.55	1.91	1.91	1.91	1.91	1.91
Hydraulic pressure (MPa)	0.6	0.6	0.6	0.6	0.6	0	0.2	0.4	0.6	0.8
Effective stress (MPa)	1.07	1.39	1.71	2.03	2.35	1.91	1.84	1.78	1.71	1.64
Fracture width (mm)	0.741	0.701	0.631	0.561	0.541	0.681	0.571	0.611	0.631	0.661

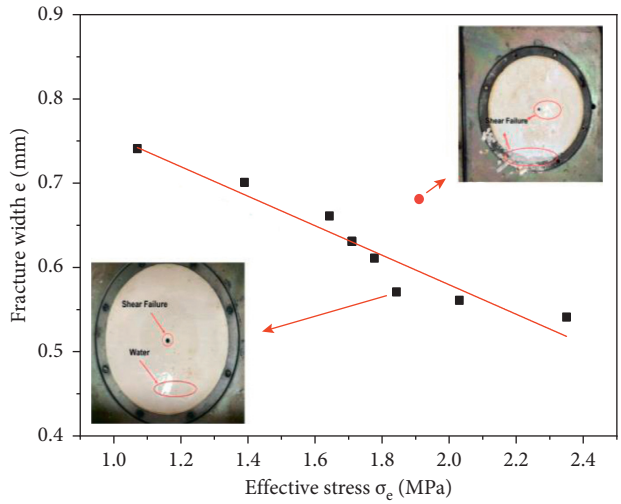

Figure 7: Fitting curve of relationship between fracture aperture and effective stress.

aperture is reduced. The shear failure material fills the fracture, making the fracture aperture open larger. Therefore, the working condition described by the red dot in the figure shows a large fracture aperture. Within the effective stress range of 1 MPa–2.5 MPa, the relationship between effective stress and fracture aperture can be obtained by using the shear seepage test data:

$$e = -0.175\sigma_e + 0.93. \tag{6}$$

From this expression, it can be deduced that the aperture of fracture tends to close with the increase of effective normal stress in a certain range. The fracture aperture decreases linearly with the increase of the effective stress; when the effective stress increases by 1 MPa, the fracture aperture closes by 0.175 mm.

3.3. Flow Rate Analysis. When the fracture aperture changes during the shear process, the fluid flow also changes. The flow rates under different normal stresses and hydraulic pressures are plotted in Figures 5 and 6, respectively. In the initial stage of shearing, the fracture aperture rapidly increases under shear dilation, which increases the area of the flow channel and increases the flow rate. At this time, the changes in the aperture of the fracture and the flow rate are very large. In the second stage of fracture dilation, the destruction of the fracture surface has an obstructive effect on the flow channel. At this time, the changes in the aperture of the fracture and the flow rate are very small. In the third stage, the aperture of the fracture under compression and shear is basically stable, and the flow rate remains near the stable value. From the test results, it is found that the normal stress controls the fracture aperture through compression, thereby affecting the fluid flow in the fracture. On the one hand, the hydraulic pressure controls the fluid flow by changing the pressure gradient in the fracture, and, on the other hand, it affects the distribution of fracture aperture and flow channels.

This paper studies the quantitative relationship between fluid flow and fracture aperture through theoretical analysis. For rock mass fractures, fluid flow is controlled by the N-S equation, and the expression is as follows [19]:

$$\frac{\partial(\rho\mathbf{u})}{\partial t} + \rho(\mathbf{u}\cdot\nabla)\mathbf{u} = \rho\mathbf{f} - \nabla P + \mu\nabla^2\mathbf{u}, \tag{7}$$

where $\mathbf{u}$ it is the velocity vector, μ is the dynamic viscosity coefficient of the fluid, P is the hydraulic pressure, $\mathbf{f}$ is the unit mass force, and ρ is the density of the fluid.

The N-S equation needs to be solved together with the mass conservation equation of the fluid. For incompressible fluids, the mass equation is [26]

$$\nabla\cdot\mathbf{u} = 0. \tag{8}$$

The hydraulic conductivity k and flow rate q are solved based on the N-S equation. Under the condition of low Reynolds number, the flow in the fracture is mainly affected by viscous force, the influence of inertial force can be neglected, and the fluid flow can be regarded as laminar flow. Due to the isotropy of radial flow, $u_z = 0$ and $u_\theta = 0$. Along the radial flow radius, the cylindrical coordinates are expressed as

$$f_r - \frac{1}{\rho}\frac{\partial P}{\partial r} + \frac{\mu}{\rho}\left(\frac{\partial^2 u_r}{\partial r^2} + \frac{\partial u_r}{r\,\partial r} - \frac{u_r}{r^2} + \frac{\partial^2 u_r}{r^2 \partial \theta^2} - \frac{2}{r^2}\frac{\partial u_\theta}{\partial \theta} + \frac{\partial^2 u_r}{\partial z^2}\right) = \frac{\partial u_r}{\partial t} + u_r\frac{\partial u_r}{\partial r} + \frac{u_\theta}{r}\frac{\partial u_r}{\partial \theta} - \frac{u_\theta^2}{r} + u_z\frac{\partial u_r}{\partial z}. \tag{9}$$

In the radial flow parallel plate model, the fracture surface is horizontal, and the unit mass force fr in the radial direction is 0. The fluid flow is a steady-state constant flow, and the time-varying acceleration ∂u/∂t is 0. The N-S equation is simplified as

$$\frac{\partial P}{\partial r} = \mu\left(-\frac{u_r}{r^2} + \frac{\partial^2 u_r}{\partial z^2}\right). \tag{10}$$

Because the magnitude of the fracture aperture b is smaller than the magnitude of the radial flow radius r, the high-order infinitesimal term can be omitted.

$$\frac{\partial P}{\partial r} = \mu\frac{\partial^2 u_r}{\partial z^2}. \tag{11}$$

The expression of u_r can be obtained by integrating equation (11):

$$u_r = \frac{\Delta P}{2\mu L}\left(\frac{b^2}{4} - z^2\right). \tag{12}$$

It can be seen from equation (12) that the flow velocity in the fracture aperture has a parabolic distribution in the normal direction, and the velocity at the central axis of the aperture is the largest. Integrating the flow velocity u_r along the z direction, the flow equation can be obtained as follows:

$$q = \frac{b^3}{12\mu}\cdot\frac{\gamma\Delta H}{(R_1 - R_2)}, \tag{13}$$

$$k = \frac{\gamma b^2}{12\mu}. \tag{14}$$

The hydromechanical behaviors are universal in rock masses, and these behaviors influence and interact with each other. The key to the hydromechanical coupling is the change in the fracture aperture. Combination with the fracture aperture is an important direction for the study of fluid flow and seepage. The hydromechanical coupling process is shown in Figure 8. The light and dark colors in the figure, respectively, indicate the positions of the initial fracture surface and the fracture surface after the change in the applied load. Figure 8(a) shows that the initial aperture of the fracture is u_0 without loading. The fluid will exert an upward force on the fracture surface in the fracture when a certain hydraulic gradient is introduced into the fracture, which will cause outward dilation to increase the fracture aperture. The change in the aperture of the fracture is u_w under the action of hydraulic pressure, and the actual aperture of the fracture is $u_0 + u_w$ (Figure 8(b)). The contact between the upper and lower fracture surfaces increases when the normal load is applied to the fracture structure, and the compression effect destroys the convex structure on the fracture surfaces. Moreover, the actual fracture aperture decreases. The change in the aperture is u_n under normal stress, and the actual fracture aperture is $u_0 - u_n$ (Figure 8(c)). The upper fracture surface produces upward displacement along the contact part, which is shear dilation, under the action of shear. The change in the aperture under shear is u_τ. The change in fracture aperture in most of the conditions is affected by the combination of shear, normal load, and hydraulic pressure. The change in the fracture aperture under the combined action is $u_w - u_n + u_\tau$, and the actual aperture of the fracture is $u_0 + u_w - u_n + u_\tau$.

In this study, the coupling relationship between stress and fluid flow is considered. Under compression, the deformation of the fracture structure surface can be ignored when compared with the variation of the fracture aperture. We combine the effective stress expression equation (1) and the fracture aperture expression equation (6) and obtain the fracture aperture expression considering the coupling effect.

$$e = -0.175\left(\sigma_n - \sigma_w\right) + u_\tau + u_0. \tag{15}$$

The initial aperture u_0 and the change of the aperture u_τ under the effect of shear dilation are mainly affected by the roughness of the fracture surface. The sum of the two items in this study is 0.93 mm. Combined with the fracture aperture (equation (15)) and the permeability coefficient (equation (14)), the coupling relationship between stress and seepage can be obtained as follows:

$$k = \frac{\gamma\left[-0.175\left(\sigma_n - \sigma_w\right)^2 + u_\tau + u_0\right]^2}{12\mu}. \tag{16}$$

As an important parameter of fluid flow, the Reynolds number is usually used to judge fracture flow regime. The expression and description of Reynolds number of radial flow and parallel flow are quite different. For parallel flows, the Reynolds number is expressed as

$$\mathrm{Re} = \frac{\rho Q}{\mu\omega}, \tag{17}$$

where ρ is fluid density, Q is flow rate, μ is dynamic viscosity, and ω is the width of seepage perpendicular to the direction of seepage. For parallel flow, ω is a fixed value, but for radial flow $\omega = 2\pi r$, and r is changing along the radial distance. Therefore, the expression of radial flow can be written as

$$\mathrm{Re} = \frac{\rho Q}{2\pi r\mu}. \tag{18}$$

It can be seen from equation (18) that the Reynolds number changes with the change of seepage radius, and the Reynolds number is closely related to hydraulic pressure. The variation of Reynolds number of fracture is studied by using the flow data obtained under different hydraulic pressure, and the flow regime of seepage in fracture is further studied. The Reynolds number along the radial direction is calculated according to the groups 6–10 of test data, which is plotted in Figure 9. It can be seen from the figure that the Reynolds number varies greatly under

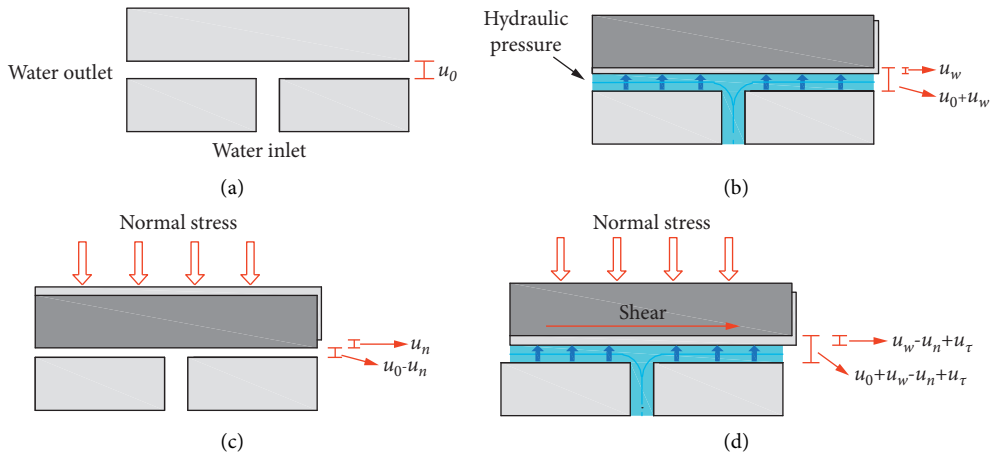

Figure 8: Hydromechanical coupling process analysis.

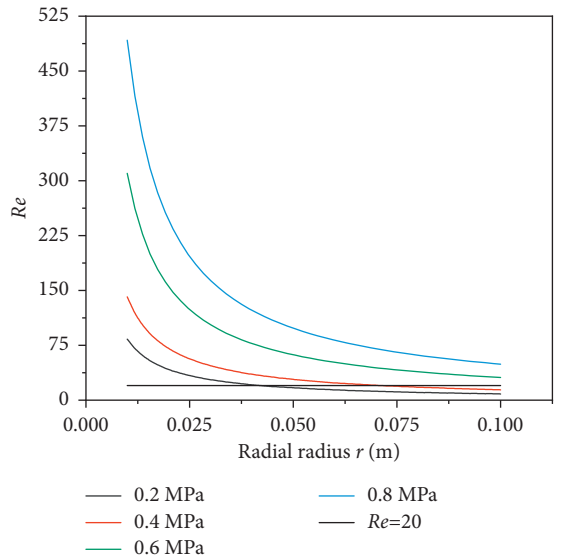

Figure 9: The variation curve of Reynolds number along radial distance under different hydraulic pressure rates.

different hydraulic pressures. At the same radial position, the Reynolds number under 0.8 MPa and 0.2 MPa hydraulic pressures differs by about 5.9 times, because the pressure gradient affects the flow rate. Because the area of circulation passage near the inner diameter is small and the area of circulation passage far from the inner diameter is large, the Reynolds number near the inlet is large and the Reynolds number far from the inlet is small. Under the same hydraulic pressure, the Reynolds number difference between the inner diameter and outer diameter of the fracture is about 20 times. The variation of Reynolds number affects the flow pattern distribution in the fracture. The Reynolds number is the ratio of inertia force to viscous force, which is usually used to judge the linear and nonlinear flow transition. The existing research conclusion is that the critical Reynolds number value range of nonlinear flow is 5–20. When the Reynolds number exceeds the critical value, the inertia force plays a leading role and the flow regime is mainly nonlinear. In order to study the radial flow state, we take the upper limit value 20 of this range as the judgment basis for the beginning of nonlinear flow, mainly to reduce the influence of the transition zone. The curve of Re = 20 is plotted in Figure 9, and the position where it intersects with different Reynolds number curves is the starting position of the linear flow. It can be found that, under high hydraulic pressure, the flow in the fracture is large and the flow along the radial direction is nonlinear flow. When the hydraulic pressure is reduced to 0.4 MPa and 0.2 MPa, the critical position of nonlinear flow and linear flow is 71 mm and 42 mm away from the inlet, and the lower the hydraulic pressure is, the closer the nonlinear flow occurs to the inlet. Under high hydraulic pressure, the parallel flow and radial flow fracture are dominated by nonlinear flow, while, under low hydraulic pressure, the parallel flow fracture is dominated by linear flow. The radial flow has the transformation of nonlinear flow and linear flow along the radial direction, and the seepage situation is more complicated than parallel flow.

3.4. Simulation of Radial Flow Velocity. In the above study, the flow regime in the macroscopic fracture was studied by means of the Reynolds number, but the distribution and maximum flow velocity in the fracture could not be shown by the experiments. Therefore, combined with the fracture aperture of 0.631 mm obtained in test 3, we established the radial flow fracture model by using COMSOL software, as shown in Figure 10. In the figure, the hydraulic pressures of the inlet were 0.2 MPa, 0.4 MPa, 0.6 MPa, and 0.8 MPa, respectively; and the water outlet hydraulic pressure was 0 MPa. In the study, the inner and outer diameters were changed, respectively, to study the seepage influence under different working conditions. As shown in Figure 11, due to the symmetry of radial flow, the cross section along the X-axis is utilized to analyze the change of the flow velocity (Figure 11).

In order to analyze the change of flow velocity along the radial direction in the fracture, the flow velocity at the positions of 0 mm, 0.1 mm, 0.3155, 0.531 mm, and 0.631 mm along the fracture aperture direction was selected as the research object. It can be seen from the figure that the fluid flow moves upwards along the water inlet. Because the fracture surface has an obstructive effect on the fluid flow, turbulence is easy to occur at the upper fracture surface, and the flow velocity is the smallest. As the fluid flows into the fracture, the flow rate gradually increases until the maximum flow rate is reached just as the water enters the fracture. As the flow continues along the radial direction, the cross-sectional area increases and the flow rate reaches a minimum at the outlet due to the continuity of the flow. To further study the flow velocity in the fracture, we took five positions in the direction of the fracture fracture, respectively, and studied the influence of the distance between the inner and outer diameters on the flow velocity through the flow velocity of these positions. The flow velocity along the radial distance from 3.5 mm to 10 mm under different hydraulic pressures is plotted in Figure 12. This distance represents the flow of water from the inlet to the fracture. Within the range of the inlet, the stratification of flow velocity occurs, but this phenomenon is not obvious because of the flow disturbance. After the fluid enters the fracture, the velocity increases. After the fluid flows into the fracture completely (after the radial distance is 4 mm), the flow velocity in the fracture is significantly different due to the vertical flow component in the initial stage of fluid flow. The fluid flow is greatly affected by the upper fracture surface. Therefore, the flow velocity decreases gradually from the lower fracture surface to the upper fracture surface, and the flow velocity of the fracture has an obvious stratification phenomenon. With the increase of the radial distance, the effect of the flow in the vertical direction is gradually decreasing, and the flow is mainly horizontal. Therefore, after the radial distance of 8 mm, the flow velocity in the fracture is basically close, and the stratification phenomenon disappears.

The flow velocity near the inner diameter fluctuates greatly, so the influence of the inner diameter on the flow velocity needs further investigation. By changing the inner diameter size from 2 mm to 8 mm, the outer diameter remains unchanged at 100 mm. The maximum flow velocity under different hydraulic pressures and inner diameters is plotted in Figure 13. It can be seen from Figure 13 that the maximum flow velocity decreases with the increase of the inner diameter. The variation of velocity increases with the increase of hydraulic pressure and decreases with the increase of inner diameter. The maximum velocity difference can be as much as three times when the inner diameter difference is 6 mm. The size of the inner diameter determines the size of the water inlet. With the increase of the inner diameter, the flow into the fracture will increase, and the seepage area of water into the fracture will also increase. It can be obtained from the downward trend of the curve in the figure that the increasing inner diameter has a greater impact on the maximum flow velocity than on the flow rate.

In this section, the fluid flow under different hydraulic pressures and different inner diameters is studied through numerical simulation, and the changes of the flow regime and flow velocity inside the fracture are analyzed. Under low hydraulic pressure, the flow changes from nonlinear to linear along the radial distance, and the flow velocity decreases gradually along the radial distance. The flow near the inner diameter of the inlet fluctuates greatly and the flow velocity in the fracture is stratified. The increase in the inner diameter will increase the flow rate into the fracture and reduce the maximum flow rate in the fracture.

3.5. Radial Flow Cubic Law. The cubic law is applied to study the relationship between flow rate and fracture aperture. The cubic law generally assumes that the fracture is an ideal smooth wall surface and that the flow rate through the fracture is proportional to the cubic power of the fracture aperture and the difference between the inlet and outlet hydraulic gradients. To simplify the calculation and use the theoretical model, we assume that the fluid in the fracture occurs at a low Reynolds number, and the influence of inertial forces in the fluid can be ignored.

The cubic law for parallel flow obtained on unit width is

$$q = \frac{e^3}{12\mu} \cdot \frac{\Delta P}{\Delta L}. \tag{19}$$

The cubic law applied to different types of fractures can be written as

$$Q = \omega \cdot q = \omega \cdot \frac{e^3}{12\mu} \cdot \frac{\Delta P}{\Delta L}, \tag{20}$$

where ω represents the width perpendicular to the seepage direction, as shown in Figure 14. The expression can be applied to different types of fractures, but the difference is that the expression of seepage width is different. For radial flow, the width perpendicular to the direction of flow changes all the time. Therefore, in order to obtain the cubic law applicable to radial flow, the key point is to obtain the expression mode of seepage width. Most of the existing studies determine the seepage width of radial flow through equivalent analysis combining mathematics and geometry, but there is a large error in the use of such expressions. According to the above research, it is found that the inner diameter and outer diameter of radial flow have a certain

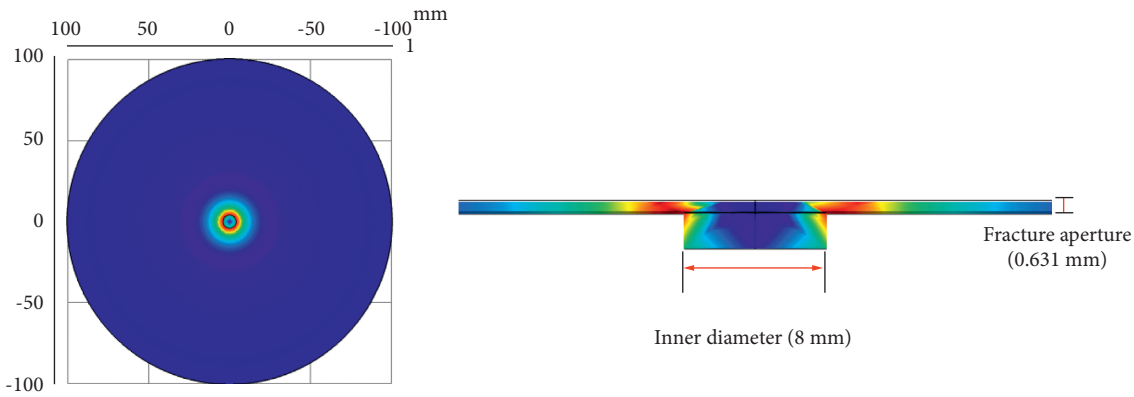

Figure 10: 3D fracture model.

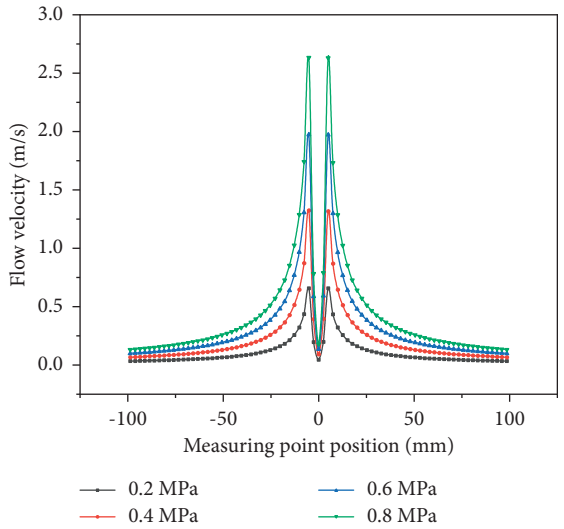

Figure 11: The variation curve of velocity along radial distance under different hydraulic pressure rates.

influence on the seepage of fracture. Based on this, the seepage width of radial flow is studied and analyzed. Using the fracture simulation method mentioned above, the fracture aperture is 0.631 mm, the hydraulic gradient is applied at the inlet, and the boundary condition applied at the outlet is 0 MPa. The inner diameter changed from 0.002 m to 0.008 m, and the outer diameter changed from 0.02 m to 0.3 m. COMSOL software was used to simulate flow through the fracture. In order to obtain the seepage width, the ratio of flow Q/q was used to get the seepage width ω. The relation diagram of seepage width under different inner and outer diameters is plotted in Figure 15.

The relationship between the inner and outer diameters and the seepage width is analyzed. As shown in the figure, the seepage width of radial flow increases with the increase of the outer and inner diameters. There is no simple linear relationship between radial flow seepage width and outer diameter, which is quite different from previous scholars who used $2\pi R_1$ or $\pi (R_1 + R_2)$ to describe the seepage width. The linear relationship underestimates the seepage width when the outer diameter is small and overestimates the effect of the seepage width with the increase of the outer diameter. We found that there is a gap between the calculated flow and the actual flow. According to the curve in the figure, we find that the power law function can be used to fit the relationship between the seepage width and the inner radius R_1, and the fitting result is as follows:

$$\omega = aR_1^b, \tag{21}$$

where a and b are the fitting parameters, and the study found that a and b are related to the inner diameter of radial flow R_2; the values of parameters a and b obtained by fitting are recorded in Table 5.

It can be clearly seen from the table that the values of parameters a and b are closely related to R_2; the value of a also increases with the increase of R_2 and the value of b shows a decreasing trend with the increase of R_2, but this change is not linear. Figure 16 is plotted from the data in the table. There is a strong nonlinear relationship between parameters a and b and parameter R_2, which shows a strong regularity; parameters a and b can be expressed as

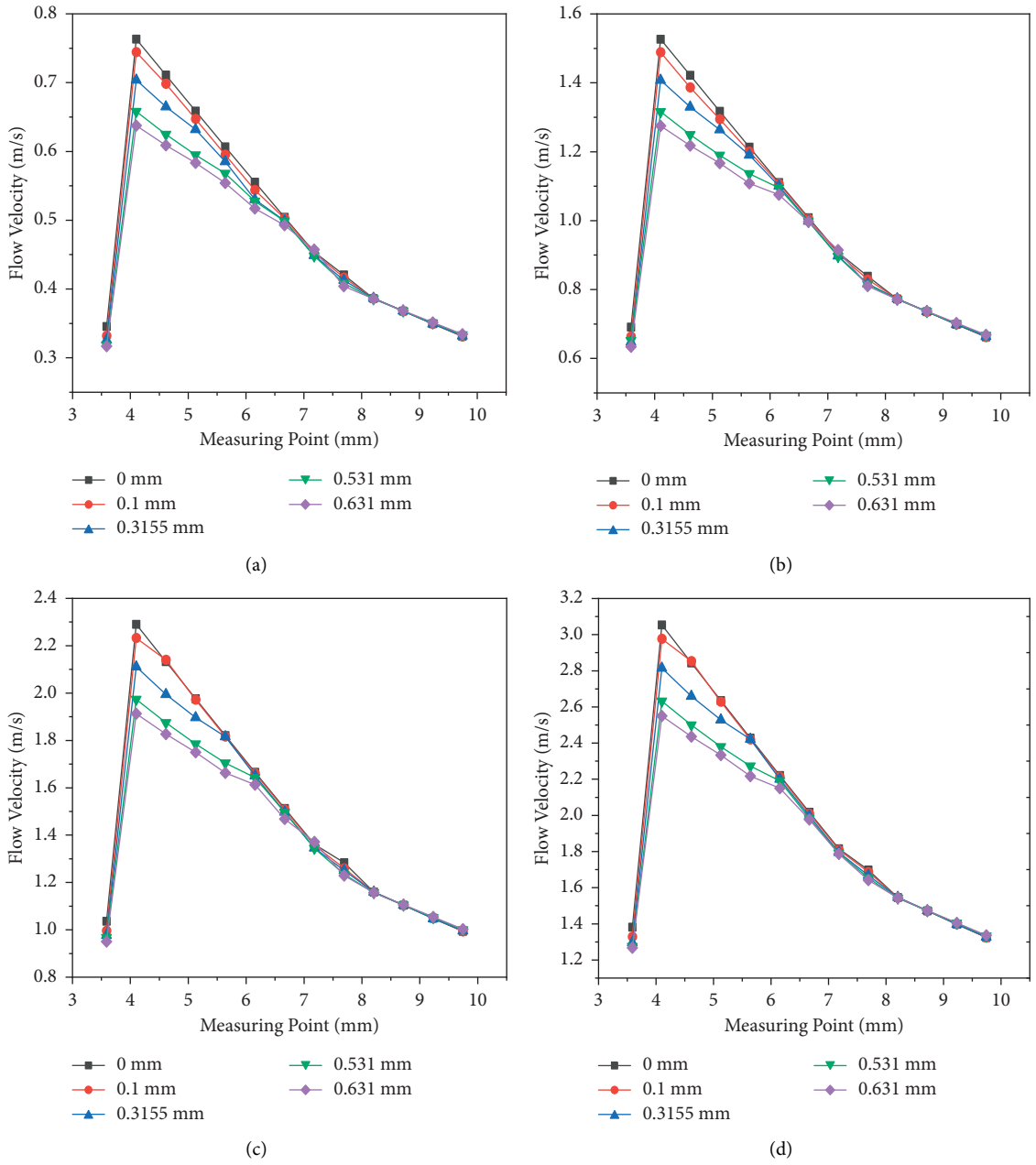

Figure 12: The curve of velocity variation along the aperture direction of fracture under different hydraulic pressure rates. (a) 0.2 MPa, (b) 0.4 MPa, (c) 0.6 MPa, and (d) 0.8 MPa.

$$a = 5.50R_2^{0.21},$$
$$b = 0.50R_2^{-0.08}. \tag{22}$$

By substituting the values of parameters a and b into equation (21), the seepage width ω can be expressed as

$$\omega = 5.50R_2^{0.21} \cdot R_1^{\left(0.50R_2^{-0.08}\right)}. \tag{23}$$

From the above analysis, it is found that the seepage width of radial flow is related to the inner and outer diameters. As shown in Figure 17, when the ratio R_1/R_2 between inner and outer diameters is constant, 40, 30, 20, and 10, respectively, it is found that there is a linear relationship between seepage width and outer diameters. With the increase of ratio R_1/R_2, the change rate of seepage width decreases, and the unit change rates of seepage width are 2.69, 3.33, 3.58, and 4.33, respectively. This shows that the inner diameter has a great influence on the fluid flow and determines the seepage width to a great extent. To sum up, the inner diameter and outer diameter of radial flow are important factors affecting the seepage width, and there is a nonlinear relationship between the seepage width and the outer diameter, so the analysis of the radial flow seepage width should be combined with the inner diameter and outer diameter (Figure 17).

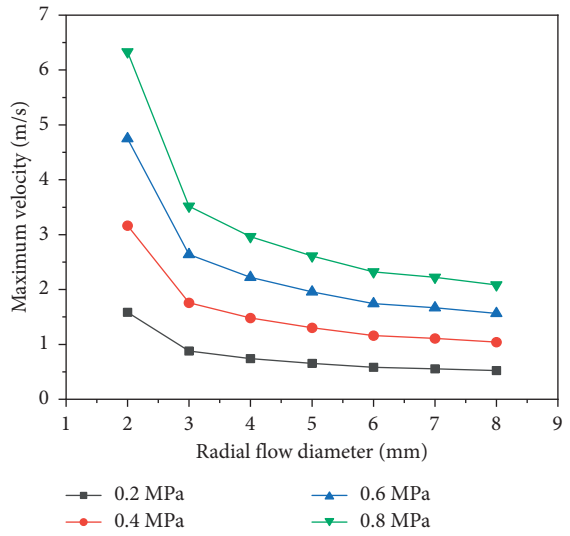

Figure 13: Maximum velocity under different hydraulic pressure rates and different inner diameters.

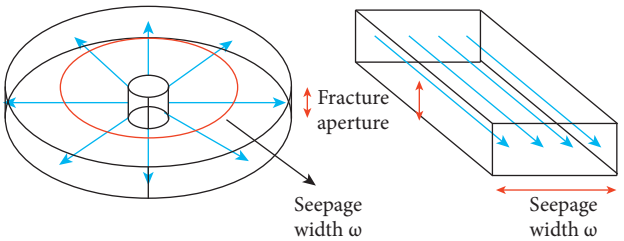

Figure 14: Radial flow and parallel flow models.

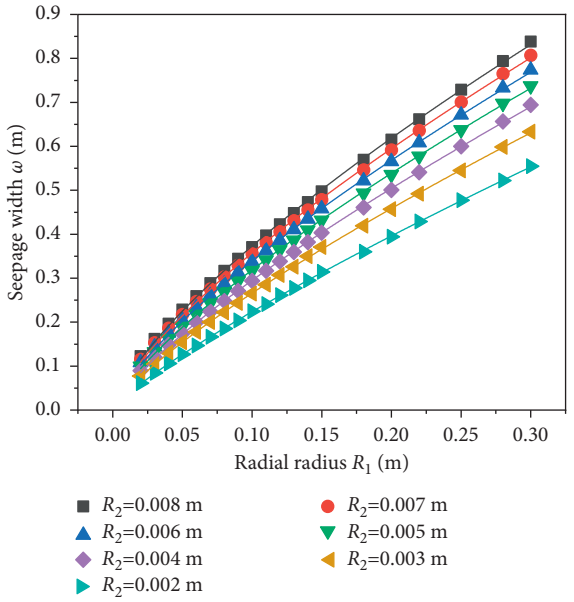

Figure 15: The fitting relation between the outer diameter of radial flow and the seepage width.

The seepage expression describing radial flow can be obtained by substituting the expression of seepage width into the flow rate calculation equation:

$$Q = 5.50R_2^{0.21} \cdot R_1^{\left(0.50R_2^{-0.08}\right)} \cdot \frac{e^3}{12\mu} \cdot \frac{\Delta P}{(R_1 - R_2)}. \tag{24}$$

Table 5: Relevant parameters of seepage width.

Radiation diameter	a	b	Degree of fitting
0.002	1.49	0.81	0.999
0.003	1.63	0.79	0.999
0.004	1.75	0.77	0.999
0.005	1.82	0.76	0.999
0.006	1.88	0.75	0.999
0.007	1.94	0.74	0.999
0.008	2	0.73	0.999

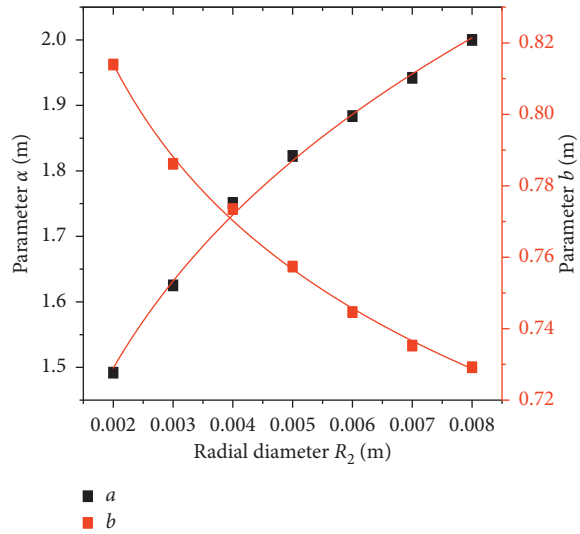

Figure 16: Fitting relation between parameters a and b and the inner diameter of radial flow.

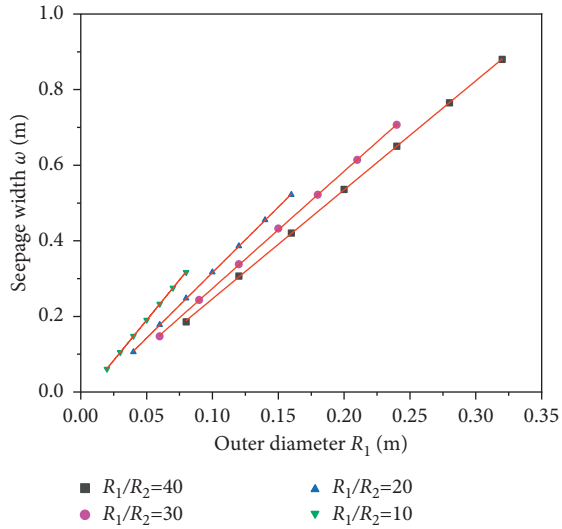

Figure 17: The variation of seepage width under fixed ratio of outer diameter to inner diameter.

The modified cubic law equation (24) combines the effects of the inner and outer diameters. Based on the parallel flow cube law, this equation describes the radial fluid flow and is theoretically accurate. Since the modified cubic law considers the size effect of the specimen, it can be applied to the description of seepage in fractures of different sizes and has a wide range of applications. The modified cubic law takes into account the area of fluid flow near the water inlet, so the seepage width of radial flow is not underestimated, which makes the result more consistent with reality. The modified cubic law is mainly applied to the analysis of seepage in fractures with smooth or low roughness surfaces.

The roughness coefficient should be used in seepage analysis of fracture surface with large roughness.

In order to verify the accuracy of the radial flow equation, we used the relationship between the measured flow rate and the fracture aperture in the shear test. In order to carry out a unified analysis under a variety of working conditions, the flow Q divided by hydraulic gradient ΔH can eliminate the influence of different hydraulic pressure in the analysis of the relationship between fracture aperture and flow. The calculated $Q/\Delta H$ and fracture aperture are presented in Table 6. Taking fracture aperture e as the abscissa and $Q/\Delta H$ as the ordinate, the relation diagram of flow fracture aperture is shown in Figure 18. The black solid point is the measured flow rate and fracture aperture under the test, and the red solid line is the fitting line obtained by using equation (24) as a function. It can be seen from the figure that the seepage points are basically maintained near the fitting line, and some points are on the line. The relationship between the curve and the points in the figure shows that the cubic relationship between the flow rate and the fracture aperture is obvious.

In order to further verify the accuracy of the radial flow cube law equation (24), we used COMSOL to simulate the fluid flow under 16 different working conditions. The hydraulic pressure increased from 0.4 MPa to 0.8 MPa, the outer radius R_1 increased from 100 mm to 300 mm, the inner radius R_2 increased from 4 mm to 8 mm, and the fracture aperture increased from 0.4 mm to 1.05 mm. The specific working conditions are shown in Table 7. This research method can verify the accuracy of the fracture aperture, hydraulic pressure, and fracture size in the equation. The flow rate in the fracture is obtained through simulation, and the corresponding parameters are put into equation (24) for calculation. We record the calculation results and simulation results in Table 7. The data in the table shows that the radial flow equation has high accuracy. Although the calculation result will be slightly larger than the simulation result with the increase of the fracture aperture and hydraulic pressure, the difference is small and within the allowable range, which is verified by the above two methods. The radial flow equation in this paper has high accuracy in describing the fracture seepage, and it is not limited by the fracture aperture and the inner and outer diameters when applied.

3.6. Analysis and Discussion. The existing shear test was conducted under low hydraulic pressure, and the outward dilation of the fracture surface by the hydraulic pressure is easily ignored. Based on the shear test, the concept of effective stress was put forward, the influence of hydraulic pressure and normal stress on the aperture of the fracture was analyzed, and the shear stress change during the whole shearing process was studied. COMSOL is used to analyze the seepage conditions under different inner and outer diameters. Roughness is an important factor affecting the curve form of shear stress change in the shear process. The shear stress process under small roughness can be divided into three segments according to the peak shear stress and the valley shear stress, which are different from the four stages of shear stress change under large roughness. In this study, by analyzing the relationship between flow rate and fracture aperture and the relationship between shear stress and fracture aperture, it is found that the change of fracture aperture plays a key role in hydromechanical behavior.

Radial flow and parallel flow have great differences in flow modes, so the seepage model suitable for parallel flow cannot be simply applied to radial flow. Along the radial direction from the inlet to the outlet, the wet circumference and seepage channel area at different locations are constantly changing. Therefore, the flow regime and flow velocity in the fracture change along the radial distance. Based on the Reynolds number expression of parallel flow, the Reynolds number expression suitable for radial flow is deduced according to the contact circumference of radial flow and fracture surface, and the flow regime of radial flow can be well analyzed. After the water enters the fracture, the seepage channel area decreases suddenly and the flow velocity increases sharply. The interaction between fluids is more obvious, and the flow state in the fracture becomes complicated. Therefore, the Reynolds number is large and the fracture is mainly within nonlinear flow regime. The flow velocity decreases as the flow area increases far away from the inlet, while the flow regime in the fracture is relatively stable. Therefore, the Reynolds number is small and the fracture is mainly within linear flow regime. The critical point of nonlinear and linear flow is closely related to the hydraulic pressure. The inner diameter affects the velocity near the entrance. The fluid flows from the inlet to the fracture, and the reaction near the fracture interferes with the surface. There is obvious velocity stratification near the inlet, and the velocity surface near the upper fracture is greater than the surface near the lower fracture surface. The inner diameter also affects the appearance of the maximum velocity in the fracture. With the increase of the inner diameter, the flow rate through the fracture increases, but the maximum velocity does decrease due to the increase of the seepage channel area.

The radial flow cube law is derived from the parallel flow cube law. Most scholars obtain the cubic law suitable for radial flow from the aspects of mathematics and geometry by equivalenting the fan flow area to the rectangular flow area or considering the flow under small angle. However, there is a gap between the calculated flow and the actual flow. By using the cubic law of parallel flow, the seepage equation of fractures per unit width can be obtained. The key to determining the radial flow cubic law equation is to determine the effective seepage width in the radial flow region. It is found that both inner diameter and outer diameter have important influence on the flow regime in the fracture. Therefore, the fluid flow of fractures under different inner and outer diameters is simulated, and the relationship between seepage width and inner and outer diameters is obtained. It is found that there is a nonlinear relationship between seepage width and inner and outer diameters, and it can be well fitted by exponential relation. The radial flow cube law can be obtained by combining the expression of seepage width with the cubic law of unit width. It is found that the radial flow cube law can be fitted well by comparing the experimental data with the radial

Table 6: Relationship between fracture aperture and flow rate under different working conditions.

Test	1	2	3	4	5	6	7	8	9	10
Hydraulic pressure (MPa)	0.6	0.6	0.6	0.6	0.6	0	0.2	0.4	0.6	0.8
Flow rate (cm^3/s)	58.20	47.83	39.00	27.33	18.96	0	10.5	17.74	39.00	61.87
Fracture width e (m)	$7.41E-4$	$7.01E-4$	$6.31E-4$	$5.61E-4$	$5.41E-4$	$6.81E-4$	$5.71E-4$	$6.11E-4$	$6.31E-4$	$6.61E-4$
$Q/\Delta H$	$9.70E-7$	$7.97E-7$	$6.50E-7$	$4.56E-7$	$3.16E-7$	0	$5.25E-7$	$4.43E-7$	$6.50E-7$	$7.73E-7$

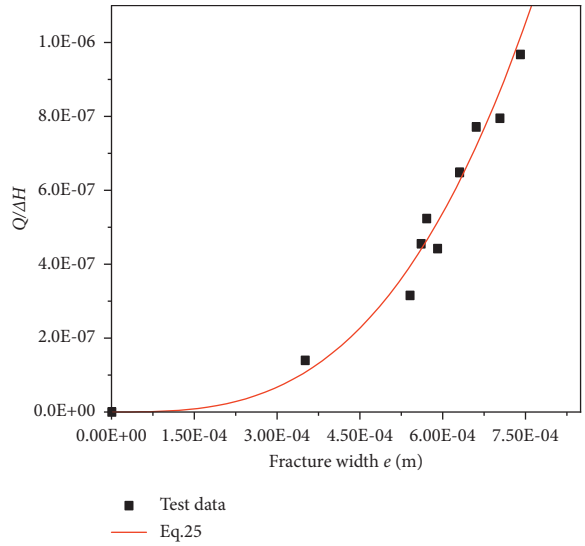

Figure 18: The measured flow and equation (15) fitting contrast analysis.

Table 7: Relationship between calculated flow and simulated flow under different working conditions.

ΔP (MPa)	0.8	0.6	0.4	0.6	0.8	0.6	0.4	0.6
R_1 (mm)	100	200	300	100	100	200	300	100
R_2 (mm)	4	6	8	8	4	6	8	8
Scheme	1	2	3	4	5	6	7	8
e (mm)	0.4				0.631			
Calculated flow (cm^3/s)	12.75	9.19	5.99	12.71	50.06	36.08	23.52	45.197
Simulated flow (cm^3/s)	13.56	9.85	6.517	13.43	50.88	36.55	24.13	48.21
Scheme	9	10	11	12	13	14	15	16
e (mm)	0.85				1.05			
Calculated flow (cm^3/s)	122.37	88.19	57.48	121.93	230.67	166.25	108.35	229.82
Simulated flow (cm^3/s)	117.62	87.23	57.59	120.01	222.56	163.58	110.62	226.54

flow cube law. The above analysis shows that the radial flow radius has a significant impact on the flow in the fracture. With the change of radial position, the velocity, flow regime, and flow rate in the fracture have changed, which are worth further study.

This paper mainly studies the radial flow based on the influence of radius and obtains the seepage law under the different radii, but there are still some limitations in the research process. When studying the effect of hydraulic pressure on fractures, the working conditions of hydraulic pressure applied are relatively insufficient, and the rule obtained is relatively simple. Secondly, we only studied the flow behaviors from the velocity and Reynolds number perspectives in the fracture but could not know the energy dissipation mechanism inside the flow and the distribution form of streamlines. These specific problems should be studied in depth in the future.

4. Conclusions

Based on the shear flow tests and numerical simulations, the characteristics of radial flow under various hydraulic pressures and radii are comprehensively investigated, and the following conclusions can be obtained:

(1) The shear process of relatively smooth fractures can be divided into three stages according to the stress characteristic points. Within the stress range of the test, the fracture aperture decreases by 0.175 mm when the effective stress increases by 1 MPa.

(2) The flow regime in the radial flow is mainly nonlinear under high hydraulic pressures. When the hydraulic pressure is reduced to 0.2 MPa and 0.4 MPa, the transition from nonlinear to linear will occur in the radial direction of the fracture. The

linear flow occurred at 42 mm and 71 mm from the inlet center, respectively.

(3) Due to the impact of the upper surface against the fluid, the velocity in the fracture is reduced, and the velocity stratification phenomenon exists within the radial distance of 8 mm. The inner diameter increases the flow rate but decreases the maximum flow velocity in the fracture. The maximum velocity difference can be as much as three times when the inner diameter difference is 6 mm.

(4) The seepage width of radial flow increases with the inner and outer diameters, exhibiting an exponential variation trend. When the ratio of the inner diameter to the outer diameter is constant, the seepage width presents a linear increase. The larger the ratio of R_1/R_2, the slower the seepage width that changes with the outer diameter. Combined with the seepage width equation, a modified cubic law is proposed for radial flow, and it describes the experimental results more accurately than the original version.

Data Availability

All data generated or used in the study are included in the article.

Conflicts of Interest

The authors declare that they have no conflicts of interest.

Acknowledgments

This work was supported by the National Natural Science Foundation of China (Grant no. 51679197), the Leadership Talent Project of Shaanxi Province High-Level Talents Special Support Program in Science and Technology Innovation (2017) (Grant no. 2013KCT-15), and the Natural Science Foundation of Shaanxi Province (Grant no. 2017JZ013).

References

[1] B. Hou, M. Chen, W. Cheng, and C. Diao, "Investigation of hydraulic fracture networks in shale gas reservoirs with random fractures," *Arabian Journal for Science and Engineering*, vol. 41, no. 7, pp. 2681–2691, 2016.

[2] X. Li, Z. Jiang, and G. G. Couples, "A stochastic method for modelling the geometry of a single fracture: spatially controlled distributions of aperture, roughness and anisotropy," *Transport in Porous Media*, vol. 128, pp. 797–819, 2019.

[3] P. Xu, B. Yu, X. Qiao, S. Qiu, and Z. Jiang, "Radial permeability of fractured porous media by Monte Carlo simulations," *International Journal of Heat and Mass Transfer*, vol. 57, pp. 369–374, 2013.

[4] M. A. Dippenaar and J. L. Van Rooy, "On the cubic law and variably saturated flow through discrete open rough-walled discontinuities," *International Journal of Rock Mechanics and Mining Sciences*, vol. 89, pp. 200–211, 2016.

[5] S. Jiang, P. Chen, M. Yan, B. Liu, H. Liu, and H. Wang, "Model of effective width and fracture conductivity for hydraulic fractures in tight reservoirs," *Arabian Journal for Science and Engineering*, vol. 45, no. 9, pp. 7821–7834, 2020.

[6] J. S. Konzuk and B. H. Kueper, "Evaluation of cubic law based models describing single-phase flow through a rough-walled fracture," *Water Resources Research*, vol. 40, 2004.

[7] H. Auradou, "Influence of wall roughness on the geometrical, mechanical and transport properties of single fractures," *Journal of Physics D: Applied Physics*, vol. 42, 2009.

[8] V. Vilarrasa, T. Koyama, I. Neretnieks, and L. Jing, "Shear-Induced flow channels in a single rock fracture and their effect on solute transport," *Transport in Porous Media*, vol. 87, pp. 503–523, 2011.

[9] C. Cao, Z. Xu, J. Chai, Y. Qin, and R. Tan, "Mechanical and hydraulic behaviors in a single fracture with asperities crushed during shear," *International Journal of Geomechanics*, vol. 18, Article ID 04018148, 2018.

[10] I. W. Yeo, M. H. de Freitas, and R. W. Zimmerman, "Effect of shear displacement on the aperture and permeability of a rock fracture," *International Journal of Rock Mechanics and Mining Sciences*, vol. 35, pp. 1051–1070, 1998.

[11] T. Koyama, N. Fardin, L. Jing, and O. Stephansson, "Numerical simulation of shear-induced flow anisotropy and scale-dependent aperture and transmissivity evolution of rock fracture replicas," *International Journal of Rock Mechanics and Mining Sciences*, vol. 43, pp. 89–106, 2006.

[12] G. Rong, J. Yang, L. Cheng, J. Tan, J. Peng, and C. Zhou, "A Forchheimer equation-based flow model for fluid flow through rock fracture during shear," *Rock Mechanics and Rock Engineering*, vol. 51, pp. 2777–2790, 2018.

[13] R. Tan, J. Chai, and C. Cao, "Experimental investigation of the permeability measurement of radial flow through a single rough fracture under shearing action," *Advances in Civil Engineering*, vol. 2019, Article ID 6717295, 2019.

[14] B. Li, Y. Jiang, T. Koyama, L. Jing, and Y. Tanabashi, "Experimental study of the hydro-mechanical behavior of rock joints using a parallel-plate model containing contact areas and artificial fractures," *International Journal of Rock Mechanics and Mining Sciences*, vol. 45, pp. 362–375, 2008.

[15] K. Matsuki, Y. Kimura, K. Sakaguchi, and A. Kizaki, "Effect of shear displacement on the hydraulic conductivity of a fracture," *International Journal of Rock Mechanics and Mining Sciences*, vol. 47, pp. 436–449, 2010.

[16] D. Casagrande, O. Buzzi, A. Giacomini, C. Lambert, and G. Fenton, "A new stochastic approach to predict peak and residual shear strength of natural rock discontinuities," *Rock Mechanics and Rock Engineering*, vol. 51, pp. 69–99, 2018.

[17] H. Kong and L. Wang, "The behavior of mass migration and loss in fractured rock during seepage," *Bulletin of Engineering Geology and the Environment*, vol. 79, pp. 739–754, 2020.

[18] S. Brown, A. Caprihan, and R. Hardy, "Experimental observation of fluid flow channels in a single fracture," *Journal of Geophysical Research: Solid Earth*, vol. 103, pp. 5125–5132, 1998.

[19] R. W. Zimmerman and G. S. Bodvarsson, "Hydraulic conductivity of rock fractures," *Transport in Porous Media*, vol. 23, pp. 1–30, 1996.

[20] C. Cao, Z. Xu, J. Chai, and Y. Li, "Radial fluid flow regime in a single fracture under high hydraulic pressure during shear process," *Journal of Hydrology*, vol. 579, Article ID 124142, 2019.

[21] M. Javadi, M. Sharifzadeh, and K. Shahriar, "A new geometrical model for non-linear fluid flow through rough fractures," *Journal of Hydrology*, vol. 389, pp. 18–30, 2010.

[22] X. Xiong, B. Li, Y. Jiang, T. Koyama, and C. Zhang, "Experimental and numerical study of the geometrical and hydraulic characteristics of a single rock fracture during shear," *International Journal of Rock Mechanics and Mining Sciences*, vol. 48, pp. 1292–1302, 2011.

[23] D. J. Brush and N. R. Thomson, "Fluid flow in synthetic rough-walled fractures: Navier–Stokes, Stokes, and local cubic law simulations," *Water Resources Research*, vol. 39, 2003.

[24] M. J. Nicholl, H. Rajaram, R. J. Glass, and R. Detwiler, "Saturated flow in a single fracture: evaluation of the Reynolds Equation in measured aperture fields," *Water Resources Research*, vol. 35, pp. 3361–3373, 1999.

[25] J. B. Walsh and W. F. Brace, "The effect of pressure on porosity and the transport properties of rock," *Journal of Geophysical Research*, vol. 89, pp. 9425–9431, 1984.

[26] L. Wang, M. B. Cardenas, D. T. Slottke, R. A. Ketcham, and J. M. Sharp Jr., "Modification of the Local Cubic Law of fracture flow for weak inertia, tortuosity, and roughness," *Water Resources Research*, vol. 51, pp. 2064–2080, 2015.

[27] X. Kong, D. Li, and D. Lu, "Transient pressure analysis in porous and fractured fractal reservoirs," *Science in China-Series E: Technological Sciences*, vol. 52, p. 2700, 2008.

[28] J. A. Barker, "A generalized radial flow model for hydraulic tests in fractured rock," *Water Resources Research*, vol. 24, pp. 1796–1804, 1988.

[29] R. Zareifard Mohammad and A. Fahimifar, "Elastic–brittle–plastic analysis of circular deep underwater cavities in a mohr-coulomb rock mass considering seepage forces," *International Journal of Geomechanics*, vol. 15, Article ID 04014077, 2015.

[30] J. Chang and Y. C. Yortsos, "Pressure transient analysis of fractal," *Reservoirs SPE Formation Evaluation*, vol. 5, pp. 31–38, 1990.

[31] P. Xu, B. Yu, S. Qiu, and J. Cai, "An analysis of the radial flow in the heterogeneous porous media based on fractal and constructal tree networks," *Physica A: Statistical Mechanics and its Applications*, vol. 387, pp. 6471–6483, 2008.

[32] Z. Changjun and H. Zhenchun, "Non-Darcy seepage modeling of groundwater flow and its simulation," in *Proceedings of the 2009 International Conference on Industrial Mechatronics and Automation*, pp. 438–441, Chengdu, China, May 2009.

[33] X. Zhang, J. Chai, Y. Qin, J. Cao, and C. Cao, "Experimental study on seepage and stress of single-fracture radiation flow," *KSCE Journal of Civil Engineering*, vol. 23, pp. 1132–1140, 2019.

[34] B. Li, Y. Jiang, T. Mizokami, K. Ikusada, and Y. Mitani, "Anisotropic shear behavior of closely jointed rock masses," *International Journal of Rock Mechanics and Mining Sciences*, vol. 71, pp. 258–271, 2014.

[35] M. S. Asadi, V. Rasouli, and G. Barla, "A bonded particle model simulation of shear strength and asperity degradation for rough rock fractures," *Rock Mechanics and Rock Engineering*, vol. 45, pp. 649–675, 2012.